Atomic clustering and magnetic moment defect in $Fe_{2.45}Mn_{0.55}Si$

1995 J. Phys.: Condens. Matter 7 2593

(http://iopscience.iop.org/0953-8984/7/13/009)

J. Phys.: Condens. Matter 7 (1995) 2593–2603. Printed in the UK

Atomic clustering and magnetic moment defect in $Fe_{2.45}Mn_{0.55}Si$

T Ersez†, S J Kennedy‡, H Kępa§ and T J Hicks†

† Department of Physics, Monash University, Clayton, Victoria 3168, Australia

‡ Australian Nuclear Science and Technology Organisation, PMB 1, Menai, NSW 2234, Australia

§ Physics Department, University of Warsaw, Poland

Received 25 November 1994, in final form 2 February 1995

Abstract. We report the first determination of the magnetic defect due to Mn in Fe_3Si using polarized neutrons. Diffuse neutron scattering was observed around the (111) and (002) Bragg peaks from measurements of a single crystal of the ordered intermetallic compound $Fe_{2.45}Mn_{0.55}Si$ at room temperature. The Mn substitutes on one of the Fe sites and this results in the loss of $0.78\mu_B$ at these sites at this composition. In addition the presence of an Mn atom reduces the moment on its eight first-neighbour Fe atoms by $0.15\mu_B$. A further defect of $0.11\mu_B$ is detected at the next magnetic site which is an Fe site partly substituted with Mn. These room-temperature results broadly support earlier findings on alloys more dilute in Mn using unpolarized neutrons with a field switched along the scattering vector. The results also reveal considerable clustering of the Mn atoms which is longer range than detected in the earlier measurements.

1. Introduction

The compounds Fe_3Si and Mn_3Si both have the DO_3-type structure and form intermediate solid solutions of $Fe_{3-x}Mn_xSi$, with $0 \leqslant x \leqslant 3$. The DO_3 structure may be described by a unit cell which consists of four cubic interpenetrating sublattices A, B, C and D with origins at the points (0, 0, 0), $(\frac{1}{4}, \frac{1}{4}, \frac{1}{4})$, $(\frac{1}{2}, \frac{1}{2}, \frac{1}{2})$ and $(\frac{3}{4}, \frac{3}{4}, \frac{3}{4})$. In the Fe_3Si crystal structure Si atoms occupy the D sites and the Fe atoms A, B and C sites. The DO_3 lattice is shown in figure 1 and the neighbour configurations for each of the A, B, C and D sites in Fe_3Si are presented in table 1. From figure 1, we see that two of the iron sites, Fe(A) and Fe(C), are equivalent with a near-neighbour (NN) configuration of 4 Fe(B) and 4 Si(D). The Fe(B) and Si(D) sites have 8 Fe(A, C) atoms as NN.

Much of the interest in the Fe_3Si system has been the selective occupation of sites when iron is substituted by other transition metals. One of the most interesting has been found in the substitution of manganese atoms to form the $Fe_{3-x}Mn_xSi$ alloy series. It has been established from NMR (Burch *et al* 1974) and neutron diffraction (Yoon and Booth 1974, 1977; Babanova *et al* 1974; Pickart *et al* 1975) studies that manganese atoms, when added to Fe_3Si, substitute selectively for Fe atoms on B sites only for Mn concentration $x < 0.75$, characteristic of $L2_1$ (Heusler) ordering. The system is ferromagnetic in this concentration range but a rapid decrease of the Curie temperature T_c and saturation magnetization occur. For $x > 0.75$, Mn atoms begin to enter A and C sites as well. The alloy exhibits a complex magnetic behaviour in this concentration range below a re-ordering temperature

Table 1. Neighbour configurations of the A, B, C and D sites given in column 1 for Fe_3Si.

No of shell	1	2	3	4	5	6	7	8
Neighbour distance expressed in lattice parameter	0.433	0.5	0.707	0.829	0.866	1	1.09	1.118
A, C	4B 4D	6A, C	12A, C	12B 12D	8A, C	6A, C	12B 12D	24A, C
B	8A, C	6D	12B	24A, C	8D	6B	24A, C	24D
D	8A, C	6B	12D	24A, C	8B	6D	24A, C	24B

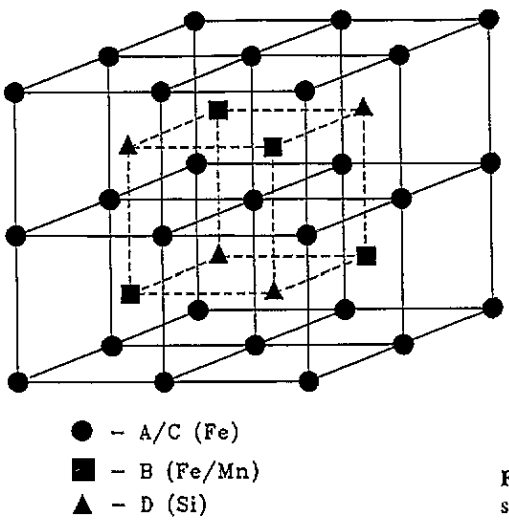

Figure 1. Unit cell of the $Fe_{3-x}Mn_xSi$ alloy system, shown with sites occupied.

T_R. From neutron diffraction measurements, Yoon and Booth (1977) proposed that the magnetic structure below T_R is rhombohedral giving antiferromagnetic components along [111] directions. The moments on the B sites in this concentration range gradually fall to zero with increasing Mn concentration, while those on the A and C sites remain constant at $\sim 0.4\mu_B$ up to $x \sim 1.5$ and then decrease slowly to zero. T_R increases to about 70 K up to $x = 1.0$ and then remains fairly constant up to $x = 1.75$. The B site becomes completely occupied by Mn at $x \sim 1.5$ (Booth 1988).

A local environment model developed by Niculescu *et al* (1983) appears to explain the systematic variations with concentration of the atomic moments and hyperfine fields in Fe_3Si and its 3d transition metal ternary alloys.

Kępa *et al* (1988a, b) have performed room temperature neutron diffuse scattering and saturation magnetization experiments on single-crystal specimens with $x = 0.164$ and $x = 0.284$ in which they observed pronounced clustering of Mn atoms on the B sublattice instead of a random distribution. Their results also suggested a pronounced decrease of the Mn magnetic moment with increasing temperature. Since single-crystal measurements are needed to determine the spin arrangements in the $Fe_{3-x}Mn_xSi$ system (because neutron powder data alone cannot be used to interpret magnetic intensities in terms of unique spin directions) we report a room-temperature polarized neutron diffuse scattering study of a single-crystal specimen with $x = 0.55$, which is just below the re-ordering temperature

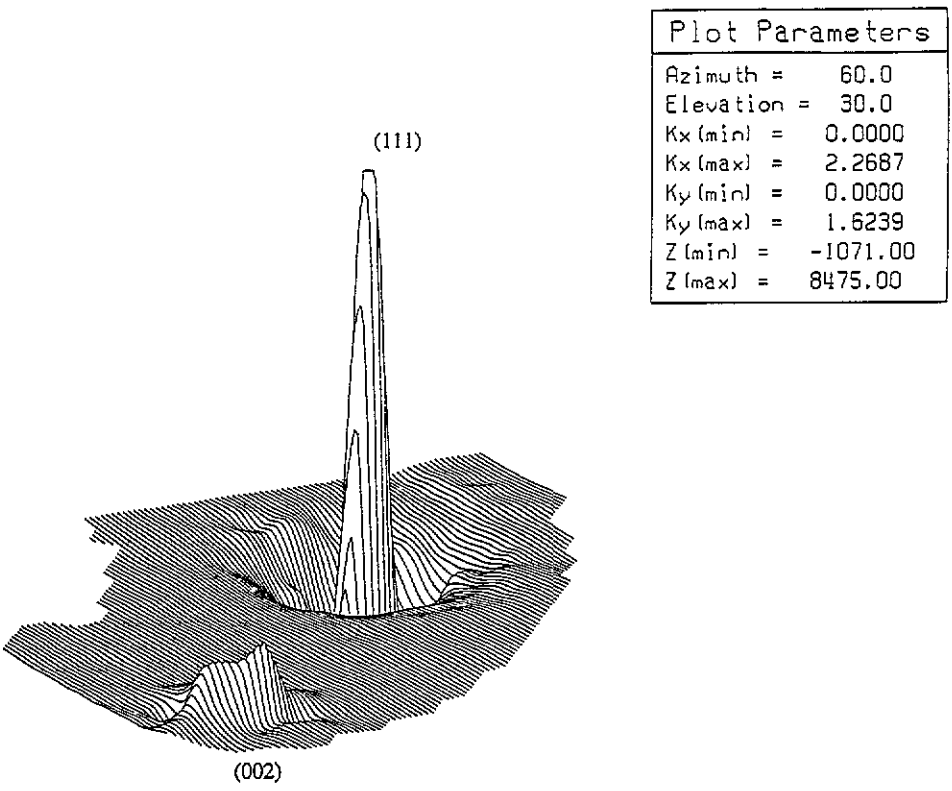

Figure 2. Surface plot of the raw difference between spin-up and spin-down scattering cross-sections.

region in composition. The Curie temperature of the specimen and its magnetic moment per formula unit, obtained from magnetization measurements, are $T_c \sim 490$ K and $\mu \sim 3.2\mu_B$ (at 4.2 K) respectively. The specimen is ferromagnetic and for this Mn composition a re-ordering phase does not exist. The results and analysis of the room temperature measurements for the $Fe_{2.45}Mn_{0.55}Si$ crystal are given in the next sections, in which the atomic distribution and the magnetic moment defect due to Mn atoms when added to Fe_3Si along with the magnitudes of the moments on the individual atomic species are presented.

2. Experimental details

The sample was a large single crystal of dimensions ($40 \times 26 \times 10$) mm^3 with the long axis along [1$\bar{1}$0] and the two other axes along [001] and [110]. The lattice parameter and composition were checked using x-ray diffraction and electron microprobe analysis. The composition was also determined from the dependence of the Curie temperature on Mn concentration, and the Curie temperature in turn was evaluated from the temperature behaviour of the intensity of the (111) Bragg peak.

The crystal is ferromagnetic at room temperature and was mounted with its long [1$\bar{1}$0] axis vertical within a c-shaped permanent magnet in a vertical field of 1.5 kOe. Neutron polarization experiments were performed on the LONGPOL spectrometer at the HIFAR Research Reactor (Lucas Heights, Australia). Monochromatic neutrons with a wavelength of 3.6 Å were used which pass through a magnetized iron polarizing filter. The iron

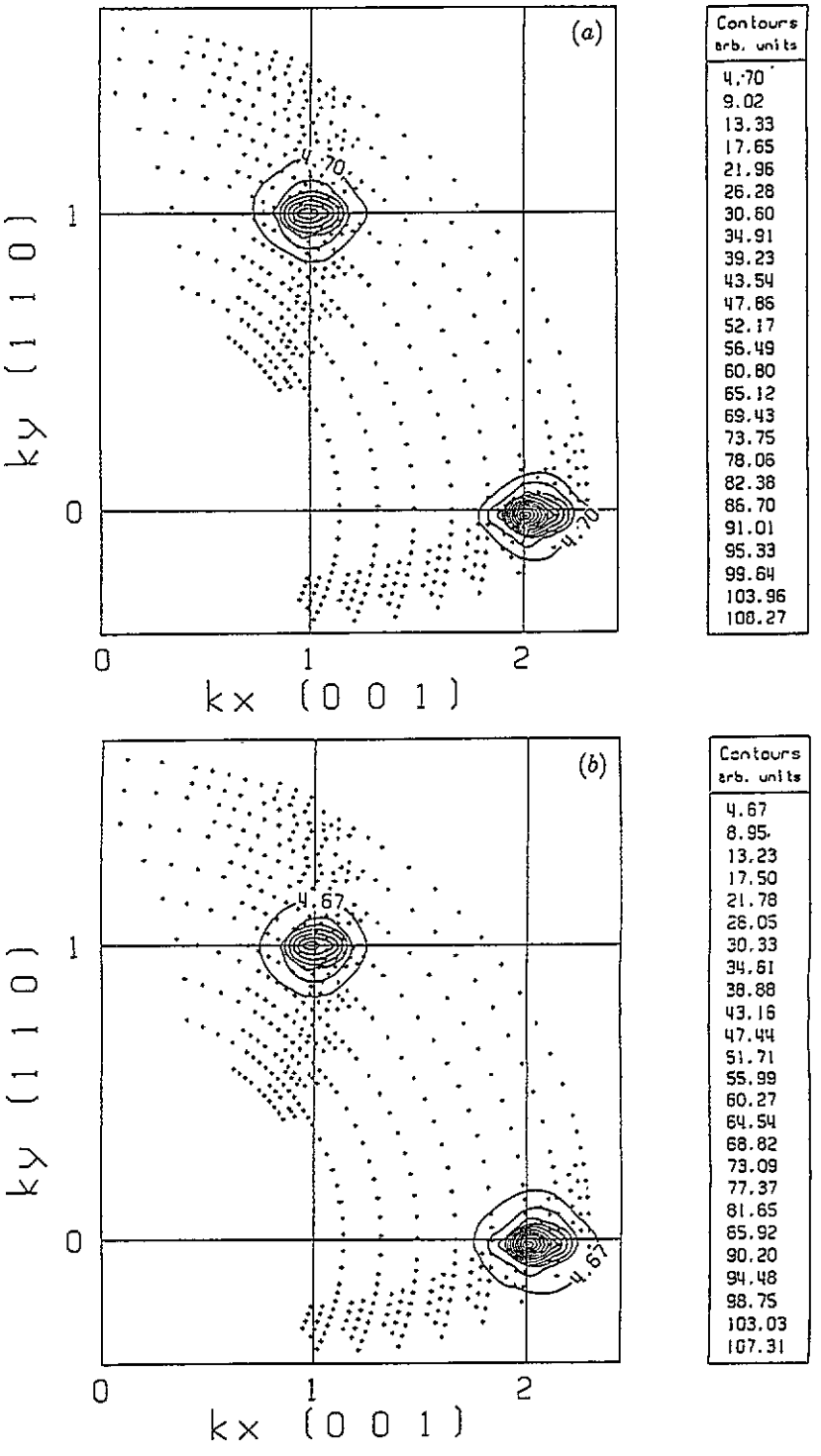

Figure 3. (a) Contour plot of the experimentally determined nuclear short-range-order function $S(\kappa)$. (b) Contour plot of the least-squares fit of equation (3) to the experimentally determined $S(\kappa)$. (c) Contour plot of the least-squares fit of the experimentally determined $S(\kappa)$ to the Clapp–Moss pair interaction model using equations (4) and (6).

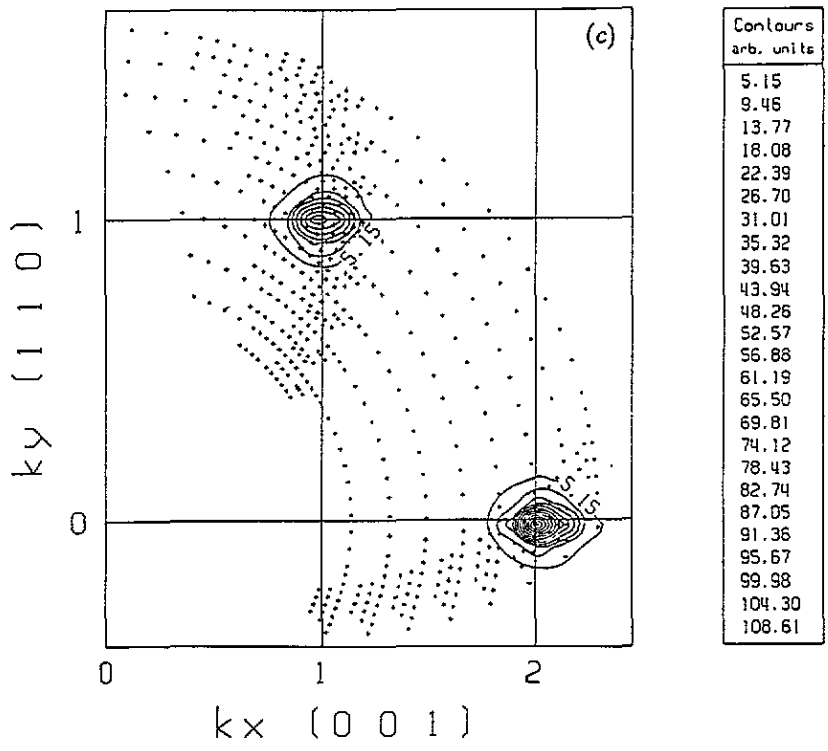

Figure 3. (Continued)

analysing filter was removed. A neutron spin flipper was used before the sample position and the instrument has eight detectors. A time-of-flight (TOF) experiment was carried out, measuring elastic scattering, by pulsing the spin flipper with a psuedo-random sequence and cross-correlating the resulting time sequence at the detector with that impressed on the spin flipper.

Background measurements were made by carefully matching the sample attenuation with an indium sample of approximately the same area. Indium is ideal to use for measuring background because of its high absorption and low scattering cross-sections. The background was subtracted from the data before carrying out further analysis. Relative detector efficiency and absolute cross-section calibration were performed by substituting a vanadium sample of similar dimensions and repeating the experiments.

Multiple scattering and absorption corrections were made by using the analytical techniques of Blech and Averbach (1965) and Sears (1975), in which the multiple scattering was appropriately apportioned between flipper on and off events.

3. Experimental results and discussion

From measurements of flipper on and off intensities for the (111) and (002) Bragg peaks and using the value of $0.7\mu_B$ for the magnetic moment of Fe on the A and C sites as reported by Yoon and Booth (1977) and also using the magnetic form factors of Fe^{2+} and Mn^{2+} from Watson and Freeman (1961), the average moment of the B site was calculated to be $1.77\mu_B$ and the polarization determined as 28%. This value of $1.77\mu_B$ is in close agreement with the value reported by Sidorenko *et al* (1976) for the composition with $x = 0.51$.

Diffuse scattering was observed around the (111) and (002) Bragg peaks. The diffuse and Bragg scattering at (111) were of opposite sign (see surface plot of the difference between raw spin-up and spin-down scattering cross-sections shown in figure 2). This is also clearly seen in the surface plot of the Fourier transform of the magnetic moment defect distribution, $M(\kappa)$, shown in figure 4. Note the absence of any significant magnetic component at the (002) position. This is due to the average magnetic moment of the B sites being approximately equivalent to twice the magnetic moment of the A and C sites.

The sign difference, observed in figure 2, for the diffuse and Bragg scattering at the (111) position is consistent with a loss of moment on the B site with addition of manganese and the nuclear structure factor being already negative at this composition. The reason for the sign difference is as follows: the (111) Bragg peak intensity is of negative sign as it is proportional to the product of the average nuclear and magnetic scattering amplitudes. The diffuse peak intensity, however, is of positive sign because it is proportional to the product of the change in nuclear and magnetic scattering amplitudes with Mn concentration (both negative). This explains the opposite signs seen at the (111) position for the Bragg and diffuse peak intensities.

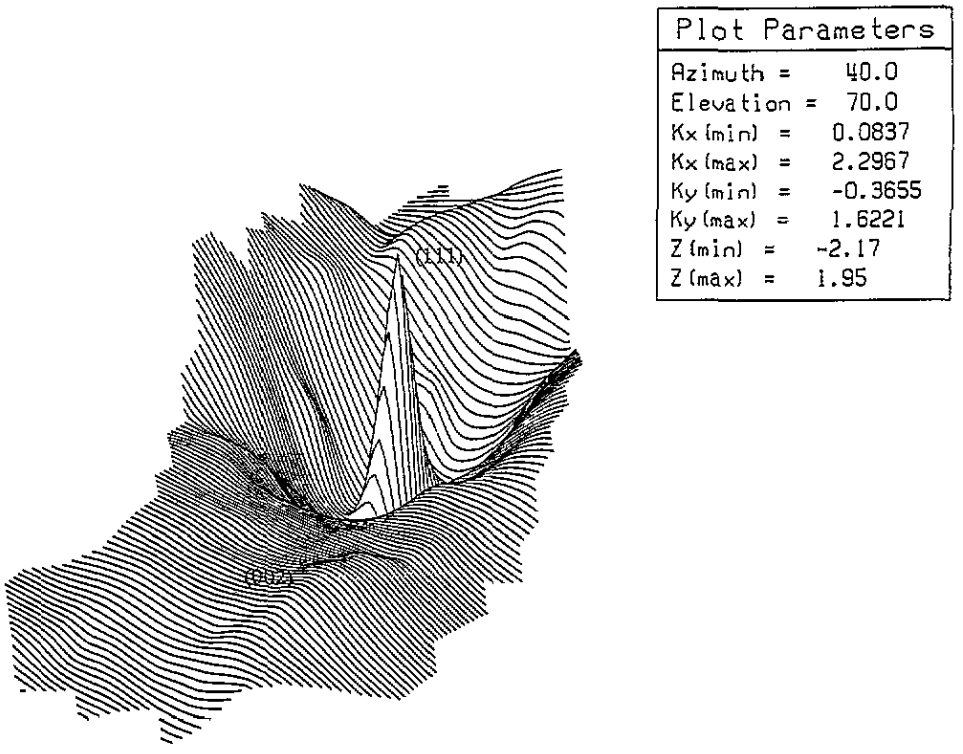

Figure 4. Surface plot of the experimentally determined Fourier transform of the magnetic moment defect distribution, $M(\kappa)$.

3.1. Nuclear diffuse scattering

The neutron diffuse cross-sections for the two spin directions can be written in the following forms

$$\left(\frac{d\sigma}{d\Omega}\right)^{\uparrow} = x(1-x)S(\kappa)\left[\left(\frac{e^2\gamma}{2mc^2}\right)M(\kappa)f(\kappa) + (b_{Fe} - b_{Mn})\right]^2 \tag{1}$$

$$\left(\frac{d\sigma}{d\Omega}\right)^{\downarrow} = x(1-x)S(\kappa)\left[\left(\frac{e^2\gamma}{2mc^2}\right)M(\kappa)f(\kappa) - (b_{Fe} - b_{Mn})\right]^2 \tag{2}$$

where c is the Mn concentration, $f(\kappa)$ the atomic form factor of both Fe and Mn, $(e^2\gamma/2mc^2) = -0.269 \times 10^{-12}$ cm $\mu_B{}^{-1}$, $(b_{Fe} - b_{Mn}) = 1.327 \times 10^{-12}$ cm is the difference of nuclear scattering amplitudes, $S(\kappa)$ is the nuclear short-range-order (SRO) function and $M(\kappa)$ the Fourier transform of the magnetic moment defect distribution.

From these two equations the total and difference cross-sections can be worked out. $S(\kappa)$ has the following form

$$S(\kappa) = \sum_{R_i} \alpha_i e^{i\kappa \cdot R_i} \tag{3}$$

where α_i are the Cowley SRO parameters (Cowley 1950), R_i are the radius vectors from the defect atom to neighbours in the ith shell and κ is the neutron scattering vector. A positive(negative) α indicates a preference for like(unlike) neighbours.

The Cowley fitting was also compared with a mean-field theory of ordering. This involved fitting the nuclear diffuse scattering to a mean-field pair-interaction model (Clapp and Moss 1966, 1968; Moss and Clapp 1968; Moss and Walker 1974). In this case the neutron scattering intensity is related to the Fourier transform of $V(\kappa)$ which is proportional to the the pair interatomic potential. For a single crystal

$$S(\kappa) = (1 + V(\kappa))^{-1}. \tag{4}$$

For small $V(\kappa)$

$$S(\kappa) = 1 - V(\kappa) + V^2(\kappa) - V^3(\kappa) + \ldots \tag{5}$$

with

$$V(\kappa) = \sum_{R_i} V(R_i) e^{i\kappa \cdot R_i} \tag{6}$$

where $V(R_i)$ is proportional to the pair interaction potential energy between an atom and the same kind of atom a distance R apart.

This model is only valid for weak interactions but nevertheless gives useful information concerning atomic ordering.

The experimental cross-section data were converted to values of $S(\kappa)$ using equations (1) and (2), which are presented in the contour plot shown in figure 3(a). These results were then least-squares fitted to equation (3) using the Cowley model to fit the diffuse scattering data with two bivariate gaussian distributions to fit the Bragg peak intensities (figure 3(b)). Theoretically $\alpha_0 = 1$ and the fit was made with parameters α_1 to α_6 (i.e. up to sixth Mn NN), the mean square error was ~0.853. Extending the fit beyond the 6th NN did not significantly improve the fit. The results of the fittings are given in table 2. A positive value for α_i indicates a preference for like NN. This condition in the sample is denoted as clustering, and a clustering of Mn atoms on B sites is indicated from the values of the Cowley parameters, broadly similar to that observed by Kępa *et al* (1988a, b) for much lower Mn concentrations.

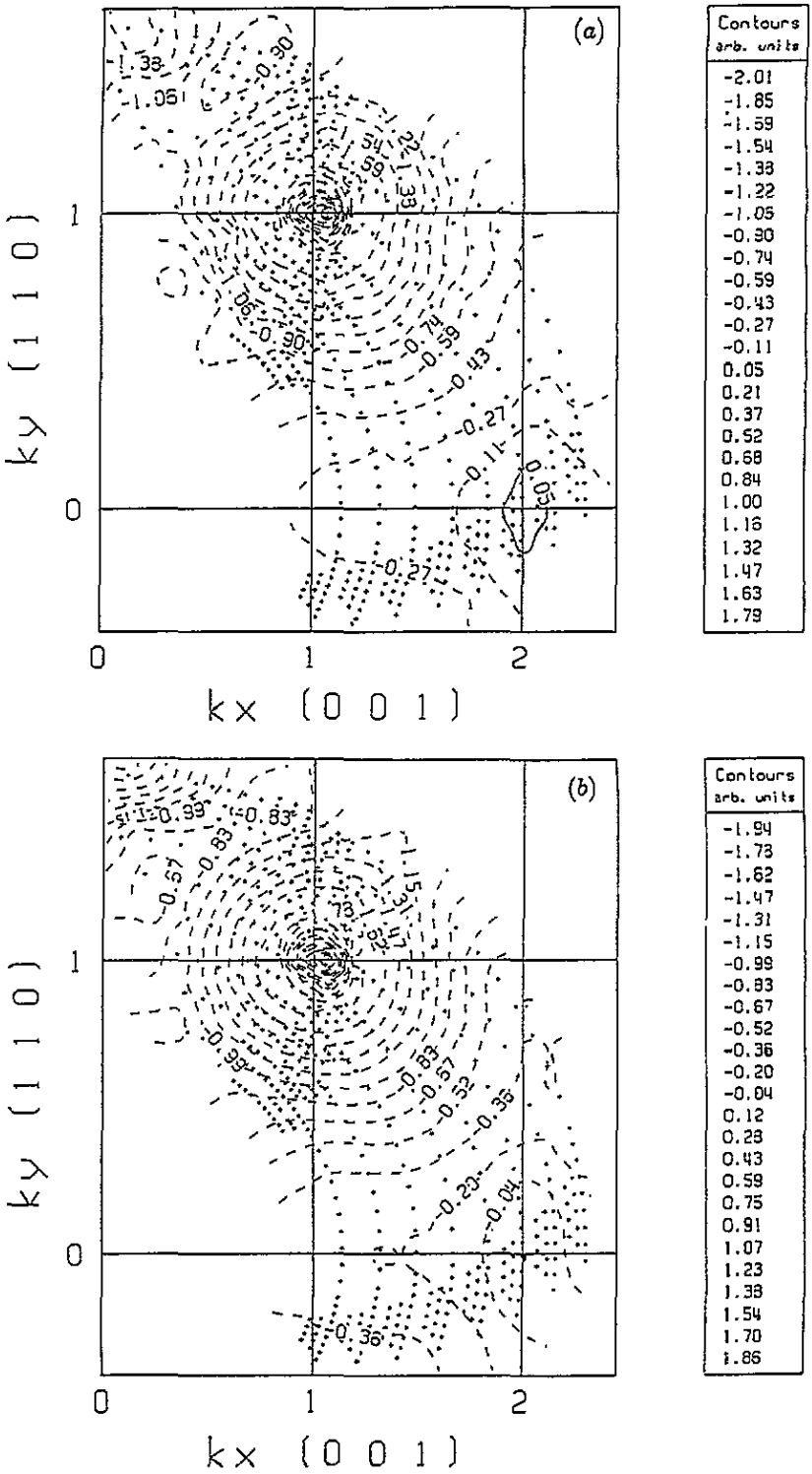

Figure 5. (a) Contour plot of the experimentally determined Fourier transform of the magnetic moment defect distribution, $M(\kappa)$. (b) Contour plot of the least-squares fit of equation (7) to the experimentally determined $M(\kappa)$.

Table 2. Cowley short-range-order and pair interaction energy parameters for $Fe_{2.45}Mn_{0.55}Si$.

Cowley SRO parameter α_i	Fit value	Standard error	Pair interaction parameters V_i	Fit value	Standard error
α_1	0.16	0.01	V_1	−0.064	0.003
α_2	0.04	0.03	V_2	−0.025	0.013
α_3	0.04	0.01	V_3	−0.00004	0.002
α_4	0.13	0.02			
α_5	0.06	0.01			
α_6	0.10	0.02			

However, the clustering observed from our results seems to be longer range compared with that observed by the above authors.

A reasonably good fit was obtained with the Clapp–Moss model using only three parameters, V_1 to V_3 shown in figure 3(c), compared with six used in the Cowley model. The mean square error was ~0.645 and the use of more parameters in the Clapp–Moss model did not show a significant improvement in the quality of the fit. The V_1 to V_3 parameters are also presented in table 2. The negative signs of the parameters in the Clapp–Moss model indicate that clustering can easily occur (Clapp and Moss 1968).

Table 3. Moment defect parameters (μ_B atom^{-1}).

m_i	Fit value	Standard error
m_0	−0.783	0.008
m_1	−0.152	0.003
m_3	−0.115	0.001
m_4	−0.039	0.001

3.2. Magnetic diffuse scattering

Fitting of a model to the magnetic diffuse scattering allows a determination of the average magnetic moments of the Mn and Fe atoms. $M(\kappa)$ is given by

$$M(\kappa) = \sum_{R_i} m_i e^{i\kappa \cdot R_i} \tag{7}$$

with R_i and κ as defined above, $m_0 = (\overline{\mu}_{Mn} - \overline{\mu}_{Fe})$, where $\overline{\mu}_{Mn}$ and $\overline{\mu}_{Fe}$ are the average moments for each of the two species on the B site and m_i the deviations of the moments at site i.

Again, using equations (1) and (2), values of $M(\kappa)$ were determined from the experimental cross-sections. These values are presented in figure 5(a) in the form of a contour plot. This set of $M(\kappa)$ data was least-squares fitted to equation (4) together with two bivariate gaussian distributions for the Bragg peaks, to yield $m_0 = (\overline{\mu}_{Mn} - \overline{\mu}_{Fe})$ and the deviations of moments m_i. The fit is shown in figure 5(b). However, the (002) peak was not well-defined and the $M(\kappa)$ data are relatively small due to the average magnetic moment of the B sites being approximately equivalent to twice those of the A and C sites. Therefore, some difficulty was experienced fitting with a gaussian distribution in the (002) region, but nevertheless, because the $M(\kappa)$ and bivariate gaussian distribution functions were independent, we were able to reliably fit our data and obtain very low error estimates

for the parameters m_0, m_1, m_3 and m_4. The 2nd NN shell of a B site is occupied by Si atoms which we have assumed as not possessing a magnetic moment, therefore $m_2 = 0$ here. However, Brown *et al* (1985) from their polarized neutron diffraction measurements on a Fe_2MnSi single crystal have noted Si atoms possess a magnetic moment of $-0.085\mu_B$. The mean square error for this fit was ~0.015. Using more parameters did not show significant improvement in the fit. Table 3 lists the moment deviation parameters which indicate that when Mn atoms are added to Fe_3Si, a loss of 0.78 μ_B occurs at the sites for which Mn atoms have substituted, for the composition with $x = 0.55$. The presence of an Mn atom also tends to reduce the moment on its eight 1st NN Fe atoms by $0.15\mu_B$. A further reduction of $0.11\mu_B$ was observed in the magnetic moment of the Fe/Mn atoms on the B sublattice due to the presence of an Mn atom on a B site in the 3rd NN shell. A very small reduction of $\sim 0.04\mu_B$ was observed in the moments of Fe atoms on 4th NN sites.

The average moment on the B sublattice may be expressed as follows:

$$\langle \mu_B \rangle = (1 - x)\langle \mu_{Fe} \rangle + x\langle \mu_{Mn} \rangle \tag{8}$$

i.e.

$$0.45\langle \mu_{Fe} \rangle + 0.55\langle \mu_{Mn} \rangle = 1.77\mu_B \tag{9}$$

where $x = 0.55$ and $\langle \mu_{Fe} \rangle$ and $\langle \mu_{Mn} \rangle$ are the average moments of Fe and Mn atoms respectively.

From our fitting procedure we have obtained

$$\langle \mu_{Mn} \rangle - \langle \mu_{Fe} \rangle = -0.78. \tag{10}$$

Solving these two equations simultaneously we have $\langle \mu_{Mn} \rangle = 1.42\mu_B$ and $\langle \mu_{Fe} \rangle = 2.20\mu_B$.

So, from our model one cannot assume that the average moment of a manganese atom on the B sublattice is still close to that of an iron atom i.e. $2.2\mu_B$ as previously assumed. Kępa *et al* (1988a, b) have suggested that the magnetic moment of Mn atoms is strongly temperature-dependent and this may remove the discrepancy between our observations with those of earlier neutron and NMR measurements which were carried out at liquid helium temperatures. Also, a slow decrease in the magnetic moment on Mn impurities in BCC Fe with increasing temperature in the range 0–700 K was observed by Mezei (1976). A similar system to $Fe_{3-x}Mn_xSi$ is the $Fe_{3-x}V_xSi$ series of compounds, in which the Fe(B) atoms are always surrounded by 8 Fe(A, C) atoms provided no atomic disorder is present. Kępa and Bednarski (1992) in their studies of $Fe_{3-x}V_xSi$ single-crystal specimens, in contrast to $(Fe, Mn)_3Si$ observed no temperature dependence in the slope of the magnetization versus V concentration.

The influence of the Mn atom on its 3rd NN has been reported previously using NMR spectroscopy by Niculescu *et al* (1983). The satellite splittings, due to the 3rd NN substitutions, observed in the NMR spectra have been explained by the above authors as resulting from Mn atoms affecting the internal fields at the resonant atom *indirectly* by reducing the average moments of 1st NN Fe atoms on A and C sites, which in turn change the local 4s spin polarization. But from the analysis of our room-temperature polarized neutron measurements we have observed the presence of Mn atoms in the 3rd NN shell to directly affect the changes in the magnetic moments on B sites as well as changes in the 1st NN moments.

4. Conclusion

The present results have revealed considerable clustering of Mn atoms on their preferred site, which appears to be longer range than detected in the earlier measurements of Kępa

et al (1988a, b) for much lower Mn concentration samples. The magnetic moment defects (produced by the Mn atoms) are primarily at the defect and the 1st and 3rd NN sites. But there is also a very small reduction in the moment of Fe atoms on 4th NN sites (~4.7 Å from the defect site). The average moments of Mn and Fe atoms on the B site at room temperature were determined as $1.42\mu_B$ and $2.2\mu_B$ respectively.

Acknowledgments

This work was supported by the Australian Institute of Nuclear Science and Engineering (AINSE) and the Australian Research Council.

References

Babanova Y E N, Sidorenko F A, Gel'd P V and Basov N I 1974 *Fiz. Metal. Metalloved.* **38** 586
Blech I A and Averbach B L *1965 Phys. Rev. A* **137** *1113*
Booth J G 1988 *Ferromagnetic Materials* vol 4 ed E P Wohlfarth and K H J Buschow (Amsterdam: Elsevier) p 247
Brown P J, Ziebeck K R A and Huntley J M 1985 *J. Magn. Magn. Mater.* **50** 169
Burch T J, Litrenta T and Budnick J I 1974 *Phys. Rev. Lett.* **33** 421
Clapp P C and Moss S C 1966 *Phys. Rev.* **142** 418
Clapp P C and Moss S C 1968 *Phys. Rev.* **171** 754
Cowley J M 1950 *J. Appl. Phys.* **21** 24
Kępa H, Hicks T J and Davis R L 1988a *Mater. Sci. Forum* **27/28** 267
Kępa H and Hicks T J 1988b *J. Physique* **49** Coll. C8 111
Kępa H and Bednarski S 1992 *J. Magn. Magn. Mater.* **104–107** 2065
Mezei F 1976 *Proc. Conf. on Neutron Scattering (Gatlinburg, TN, USA)* vol 2 670
Moss S C and Clapp P C 1968 *Phys. Rev.* **171** 764
Moss S C and Walker R H 1968 *J. Appl. Crystallogr.* **8** 96
Niculescu V, Burch T J and Budnick J I 1983 *J. Magn. Magn. Mater.* **39** 223
Pickart S, Litrenta T, Burch T J and Budnick J I 1975 *Phys. Lett.* **53A** 321
Sears V F 1975 *Adv. Phys.* **24** 1
Sidorenko F A, Vereshchagin Yu A, Babanova E N, Ryzhenko B V and Gel'd P V 1976 *Sov. Phys.–JETP* **43** 325
Watson R E and Freeman A J 1961 *Acta Crystallogr.* **14** 27
Yoon S and Booth J G 1974 *Phys. Lett.* **48A** 381
Yoon S and Booth J G 1977 *J. Phys. F: Met. Phys.* **7** 1079